Viscid/Inviscid Interaction Analysis of Subsonic Turbulent Trailing-Edge Flows

Mark Barnett* and Joseph M. Verdon†
United Technologies Research Center, East Hartford, Connecticut

Subsonic turbulent flow past airfoil trailing edges is studied using a finite Reynolds number viscid/inviscid interaction model in which the flow in the outer or inviscid region is governed by the equations of linearized potential flow theory, while that in the inner or viscous region is governed by Prandtl's boundary-layer equations. The effects of turbulence are represented using an algebraic turbulence model based on the eddy-viscosity concept. The flow in the vicinity of the local strong interaction is determined by iteratively matching the solutions in the inviscid and viscous regions using a quasi-simultaneous coupling procedure. Results are presented illustrating the effects of airfoil thickness and loading on the detailed turbulent mean-flow behavior in the trailing-edge/near-wake region, including a comparison between present predictions and available experimental data.

Introduction

THE design of efficient airfoils requires an understanding of the flow in the neighborhood of the trailing edge, where adverse pressure gradients can lead to boundary-layer separation. The penalties incurred because of trailing-edge separation are usually an increase in drag and a reduction in lift; its onset generally determines the upper limit of the efficient operation of an airfoil. It is therefore important to be able to predict airfoil trailing-edge flows so that the factors contributing to separation can be understood clearly and perhaps controlled.

Flows of practical interest around airfoils usually occur at Reynolds (*Re*) numbers that are sufficiently high to enable the flow to be divided conceptually into two regions: an "inner" dissipative region consisting of the boundary layer and wake, and an "outer" inviscid region. The principal interaction between the flows in the viscid and inviscid regions arises from the viscous displacement effect, which leads to a thickened, semi-infinite equivalent body with corresponding changes in surface pressure. If the interaction is "weak," i.e., the viscous effect on the surface pressure is small, then the complete flow problem can be solved sequentially. However, the flow over an airfoil involves both the weak interaction arising from standard displacement and wake curvature effects and local strong viscid/inviscid interactions caused, for example, by viscous-layer separation, shock/boundary-layer interactions, and trailing-edge/near-wake interactions. Such features lead to a breakdown of the traditional weak interaction solution procedure. The concept of an inner viscous region and an outer inviscid region still holds, but a solution for the complete flowfield must be determined by allowing for a mutual interaction between the solutions for the outer inviscid and the inner viscous regions.

In this article, an analytical procedure based on finite Reynolds number viscid/inviscid interaction theory is presented for predicting the subsonic turbulent flow past an airfoil trailing edge. The present effort is a continuation of the work reported in Refs. 1 and 2, where subsonic laminar flows were considered. The approach taken employs an interacting boundary-layer model in which the flow in the outer inviscid region is assumed to be potential and that in the inner region is assumed to be governed by Prandtl's boundary-layer equations written in similarity-type (Levy-Lees) variables. Inverse solutions to the finite-difference viscous-layer equations are dtermined using a superposition procedure particularly convenient for continuing boundary-layer solutions into an asymmetric wake. The solutions in the inviscid and viscous regions are matched through a quasi-simultaneous coupling procedure,[3,4] using global iteration to obtain a converged result for the complete flowfield. The use of a quasi-simultaneous coupling procedure represents a departure from the semi-inverse procedure employed in our earlier studies[1,2] and offers improvements in both computational efficiency and robustness.

Our intention is to provide an accurate and dependable numerical scheme for predicting strong trailing-edge interactions and to elucidate turbulent mean-flow behavior in airfoil trailing-edge/near-wake regions. Therefore we have attempted to obtain viscid/inviscid interaction solutions on highly refined numerical grids by using a rather stringent convergence criterion for the global interaction procedure. To demonstrate this scheme, turbulent mean-flow solutions will be presented for a range of symmetric and asymmetric wedge-shaped trailing-edge geometries. Also, present predictions will be assessed through a comparison with the benchmark experimental data obtained by Viswanath and Brown.[5]

In Refs. 1 and 2, solutions are presented for subsonic laminar attached and separated trailing-edge flows. In particular, separated flow results are presented in which local symmetric reverse-flow regions extend over 20% of the airfoil chord and one-sided reverse-flow regions (adjacent to the airfoil suction surface) extend over 10% of the airfoil chord. We mention also the related studies, based on the asymptotic triple-deck ($Re \to \infty$) model by Smith,[6,7] who determined numerical solutions for a separated flow past symmetric and asymmetric airfoil configurations and was the first to demonstrate that one-sided closed laminar separation bubbles at a loaded subsonic trailing edge could be predicted using viscid/inviscid interaction concepts. Later, Elliott and Smith[8] determined corresponding solutions for supersonic trailing edges. In addition, Veldman,[9] Veldman and Lindhout,[10] Melnik and Brook,[11] and Cebeci et al.[12] have obtained results for laminar and turbulent flows over airfoils using finite-*Re* interacting boundary-layer models similar to that employed here.

Received June 9, 1986; presented as Paper 87-0457 at the AIAA 25th Aerospace Sciences Meeting, Reno, NV, Jan. 12–15, 1987; revision received Feb. 4, 1987.

*Associate Research Engineer, Computational Fluid Mechanics Research. Member AIAA.

†Principal Scientist, Computational Fluid Mechanics Research. Associate Fellow AIAA.

The numerical results reported herein demonstrate that, as expected, turbulence strongly influences the behavior of the mean flow in the trailing-edge/near-wake region of loaded airfoils, particularly with regard to the separation of the viscous layer. The present results indicate that such flows remain attached to the airfoil surface over a much wider range of airfoil geometries and flow conditions than those determined in Refs. 1 and 2 for high-Reynolds number laminar flows.

Problem Description and Formulation

In the following discussion, all flow variables and spatial coordinates are dimensionless. Lengths have been scaled with respect to the length of the airfoil, density, velocity, and viscosity with respect to their freestream values, pressure with respect to twice the freestream dynamic pressure, and temperature with respect to the square of the freestream speed divided by the specific heat at constant pressure. We consider the high Reynolds number adiabatic turbulent flow, with negligible body forces, of a perfect gas with constant specific heats, linear viscosity law, and unit molecular and turbulent Prandtl numbers around an airfoil. As shown in Fig. 1, the flow is two-dimensional and subsonic ($M<1$), with freestream velocity in the positive x direction. The airfoil is thin and slightly cambered, and it is situated at a small angle of attack relative to the freestream direction. Viscous effects are concentrated in relatively thin layers adjacent to the airfoil surfaces, which merge into a thin wake. The position of the upper and lower surfaces of the airfoil and wake displacement body are defined by

$$\begin{aligned} y_\pm(x) &= h_\pm(x) \pm \delta_\pm(x) \quad \text{for } x\in[0,1] \\ &= h_W(x) \pm \delta_\pm(x) \quad \text{for } x>1 \end{aligned} \tag{1}$$

where h_+ and h_- define the locations of the upper and lower surfaces of the airfoil, h_W defines the location of the reference wake streamline, and $\delta_\pm>0$ are the displacement thicknesses of the upper and lower viscous layers. Note that in Fig. 1 the symbols $\mathcal{S}$, $\mathfrak{D}$, and $\mathcal{W}$ refer to the airfoil surface, the displacement surface, and the reference wake streamline, respectively. The latter is an arbitrary curve that emanates from the trailing edge of the airfoil and lies within the actual viscous wake.

If the outer inviscid flow is assumed to be isentropic and irrotational, then a velocity potential $\Phi=x+\phi$ exists where the disturbance potential $\phi\ll 0(1)$ can be determined by the methods of linearized potential-flow theory. The flow in the inner or viscous region is assumed to be governed by Prandtl's boundary-layer equations which, to within the order of approximation considered here, can be solved in terms of coordinates parallel (x) and normal (y) to the freestream direction. The effects of turbulence are incorporated by using the algebraic eddy-viscosity model described in Refs. 13 and 14 and introducing simple modifications to this model to permit the calculation of local separated regions and asymmetric wake flows.

In the present analysis, viscous displacement effects at the trailing edge are regarded as strong, while wake curvature effects are regarded as weak. Thus, iterative solutions of the coupled inviscid and viscous equations will be determined repeatedly to obtain a converged solution that accounts for strong displacement interactions, and the resulting solution will then be corrected to account for wake curvature effects. In the quasi-simultaneous coupling procedure used in solving the strong-interaction problem, the viscid and inviscid solutions are coupled at each streamwise station on the airfoil and in the wake. This leads to a relatively fast convergence of the global viscid/inviscid iteration scheme.

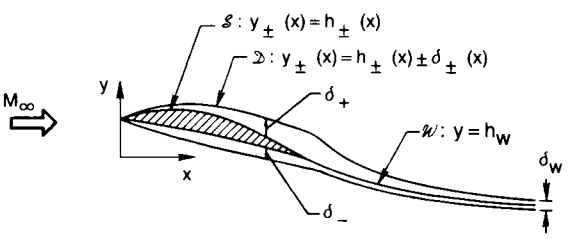

Fig. 1 High Reynolds number flow around a thin airfoil.

The Inviscid Region

The disturbance potential is determined subject to the conditions of flow tangency at the airfoil displacement surface, i.e.,

$$\phi_y|_{y=0^\pm} = [h_\pm(x) \pm \delta_\pm(x)]' \quad \text{for } x\in[0,1] \tag{2}$$

and jump conditions on normal velocity and pressure across the wake, i.e.,

$$[\phi_y] = \delta_W'(x) \text{ and } [p] = \kappa(x)[\delta_W(x)+\theta_W(w)] \quad \text{for } x>1,\ y=0 \tag{3}$$

Here the prime denotes differentiation, the boldface brackets denote the difference (upper minus lower) in a quantity across the wake, $p=-\phi_x$ is the disturbance pressure, δ_W and θ_W are the displacement and momentum thicknesses, respectively, of the complete wake, and κ is the curvature (positive—concave upwards) of the reference wake streamline. The freestream pressure is $(\gamma M_\infty^2)^{-1}$ where γ is the specific heat ratio of the fluid.

A solution for $\phi(x,y)$ can be determined using Cauchy's integral formula. It follows that the first-order pressure acting on the airfoil surface is given by

$$p(x,0^\pm) = p_D(x,0^\pm) \pm [p_{WC}^A(x)]/2 \qquad \text{for } x\in[0,1] \tag{4}$$

wher the superscripts (+) and (−) refer to the upper and lower surfaces, respectively, of the airfoil displacement body, $p_D(x,0^\pm)$ is the first-order surface pressure due to displacement (geometric + viscous) effects, and $[p_{WC}^A]$ is the jump in the pressure across the airfoil due to wake curvature. The terms on the right-hand side of Eq. (4) are evaluated using the following expressions:

$$\begin{aligned} \pi(1-M_\infty^2)^{1/2} p_D(x,0^\pm) &= -\oint_0^\infty \frac{D_T'(\zeta)}{x-\zeta}\,d\zeta \\ &\pm \frac{1-x^{1/2}}{x}\oint_0^1 \frac{D_C'(\zeta)}{x-\zeta}\left[\frac{\zeta}{1-\zeta}\right]^{1/2} d\zeta \end{aligned} \tag{5}$$

$$\oint_0^1 \frac{[p_{WC}^A(\zeta)]}{x-\zeta}\,d\zeta = -\int_1^\infty \frac{\kappa(\zeta)[\delta_W(\zeta)+\theta_W(\zeta)]}{x-\zeta}\,d\zeta \tag{6}$$

where the symbol $\oint$ denotes a Cauchy principal-value integral, $D_T=(y_+-y_-)/2$ is one-half of the displacement-body thickness, and $y=D_C=(y_++y_-)/2$ defines the location of the displacement-body camber line. In Eq. (6), the wake curvature κ is taken to be the curvature of the inviscid wake camber line as determined from the strong-displacement-interaction inviscid solution; i.e.,

$$\kappa(x) = D_C''(x) = \frac{(1-M_\infty^2)^{1/2}}{2\pi}\frac{d}{dx}\int_0^1 \frac{[p_D(\zeta)]}{x-\zeta}\,dy, \quad x>1 \tag{7}$$

The Viscous Layer

To facilitate the numerical resolution of the viscous-layer equations, we first introduce Prandtl's transformation, i.e.,

$$\tilde{y}_{\pm} = \pm Re^{1/2}(y - h_{\pm}) \qquad \tilde{v}_{\pm} = \pm Re^{1/2}(v - uh'_{\pm}) \tag{8}$$

where $h_+ = h_- = h_W$ for $x > 1$, u and v are the velocity components in the x and y directions, and the scaled normal coordinate $\tilde{y}$ and normal velocity component $\tilde{v}$ are positive along the outward normal to the x axis, and then recast the viscous equations in terms of similarity-type variables. Thus with

$$\xi = \xi_I + \int_{x_I}^{x} \rho_e \mu_e u_e g \, dx, \qquad \eta = \frac{u_e}{\sqrt{2\xi}} \int_0^{\tilde{y}} \rho \, d\tilde{y} \tag{9}$$

$$F = \frac{u}{u_e}, \qquad V = 2\xi \left[F \frac{\partial \eta}{\partial x} + \rho \tilde{v} \sqrt{Re} (2\xi)^{-1/2} \right] \Big/ \frac{d\xi}{dx} \tag{10}$$

the viscous equations can be written in the form

$$2\xi \frac{\partial F}{\partial \xi} + \frac{\partial V}{\partial \eta} + F = 0 \tag{11}$$

$$2\xi F \frac{\partial F}{\partial \xi} + V \frac{\partial F}{\partial \eta} + \beta(F^2 - 1) - \frac{\partial}{\partial \eta}\left(\ell \frac{\partial F}{\partial \eta} \right) = 0 \tag{12}$$

where

$$\beta = \frac{2\xi}{u_e} \frac{du_e}{d\xi} \left(1 + \frac{u_e^2}{2T_e} \right) = \frac{2\xi}{M_e} \frac{dM_e}{d\xi} \tag{13}$$

$$\ell = \rho\mu(1 + \gamma_T e)/(\rho_e \mu_e g) \tag{14}$$

For convenience, the subscripts (+) and (−) have been eliminated from Eqs. (9-14). Also, the subscript e refers to the edge of the viscous layer, ρ and μ are the fluid density and viscosity, respectively, γ_T is a streamwise intermittency factor which here will be assumed simply to be unity, e is the turbulent eddy viscosity, and the function $g(x)$ will be defined later in terms of the eddy viscosity. This function is included in the definition of ξ to maintain a nearly constant η value at the edge of the viscous layer. Fluid properties at the edge of the viscous layer (i.e., inviscid properties at the displacement suface $\mathfrak{D}$ are determined from Bernoulli's equation and the isentropic relations for a perfect gas. Note that as a consequence of our original assumptions, the total enthalpy is constant throughout the field.

The boundary conditions on F and V are as follows: $F \to 1$ as $\eta \to \infty$, $F = V = 0$ for $\eta = 0$, $0 \le \xi \le \xi_{TE}$, and $V = 0$ for $\eta = 0$, $\xi > \xi_{TE}$. The displacement and momentum thicknesses of the viscous layer must be evaluated from the upper- and lower-surface viscous solutions. It follows from the standard definitions that

$$\rho_e u_e \delta \left(\frac{Re}{2\xi} \right)^{1/2} = \int_0^{\infty} \left[1 - F + \frac{\gamma - 1}{2} M_e^2 (1 - F^2) \right] d\eta \tag{15}$$

and

$$\rho_e u_e \theta \left(\frac{Re}{2\xi} \right)^{1/2} = \int_0^{\infty} (1 - F) F \, d\eta \tag{16}$$

The displacement and momentum thicknesses δ_W and θ_W of the complete wake are then equal to $\delta_+ + \delta_-$ and $\theta_+ + \theta_-$, respectively. Finally, the shear stress or friction coefficient in the viscous layer is given by

$$C_f = u_e^2 \left(\frac{2}{\xi Re} \right)^{1/2} \rho\mu \frac{\partial F}{\partial \eta} \tag{17}$$

after nondimensionalizing the shear by the freestream dynamic pressure.

Turbulence Model

At high Reynolds number, the flow in the viscous layer usually undergoes a transition from laminar to turbulent near the leading edge of an airfoil. In the present study, we simulate the effects of turbulence on the mean flow by employing the eddy-viscosity model developed by Cebeci and Smith[13] for airfoil boundary layers and subsequently modified by Cebeci et al.[14] for symmetric wake flows. In this model, the turbulent boundary layer is viewed as consisting of two distinct regions, an inner one and an outer one. The eddy viscosity in the inner and outer regions is given (in terms of Levy-Lees variables) by

$$e = e_i = 0.16 D^2 (2\xi Re)^{1/2} \rho^2 \tilde{\theta}^2 \mu^{-1} \left| \frac{\partial F}{\partial \eta} \right| \qquad \text{for } \eta < \eta_1$$

$$= e_0 = 0.0168 \rho \mu^{-1} (2Re)^{1/2} \left| \int_0^{\infty} \frac{1 - F}{\rho} \, d\eta \right| \qquad \text{for } \eta \ge \eta_1 \tag{18}$$

respectively, where D is the van Driest damping factor, η_1 is defined as the smallest value of η for which $e_0 = e_i$, and $\tilde{\theta} = \int_0^{\eta} d\eta/\rho$. In the present application, the maximum value of the friction coefficient at each streamwise station of the boundary layer is used to determine D, rather than the value at the solid surface. This avoids spurious oscillations in the calculated skin-friction coefficients (i.e., C_f at $\eta = 0$) that would otherwise arise near boundary-layer separation and reattachment points.

In the turbulent wake, the inner region is subdivided further into two parts:

$$e = e_w = 0.4 \frac{\rho}{\rho(\eta_c)} \frac{\mu(\eta_c)}{\mu} \exp\left[\frac{u_e F(\eta_c)}{2.75 u_{\tau_E}} - 2.08 \right] \quad \text{for } 0 \le \eta < \eta_2$$

$$= e_i \quad \text{for } \eta_2 \le \eta < \eta_1 \tag{19}$$

where η_c is defined in Ref. 14 and $u_{\tau_E} = \sqrt{C_{f_w}/2\rho_w}$ is the shear velocity at a cusped trailing edge or a specified location upstream of a wedge-shaped trailing edge, or, if the flow separates, at a point upstream of the separation point. The value of η_2 is determined from the condition that $e_w = e_i$ at $\eta = \eta_2$. For $\eta_2 \le \eta < \eta_1$, the first of Eqs. (18) is applied with $D = 1$. To prevent e_w from exceeding e_0 at large distances downstream of the trailing edge, once $e_w = e_0$ the eddy viscosity for larger values of ξ is taken to be the local value of e_0 across the entire viscous layer.

Since the foregoing model was developed only for symmetric wakes, a modified version is applied herein to compute asymmetric wake flows; i.e., the values of e_w, e_i, and e_0 are determined by referring all quantities referenced to the wake centerline in Ref. 14 to the locus of minimum streamwise velocity. In general, this leads to a small discontinuity in the eddy viscosity which disappears with increasing distance downstream from the airfoil. Finally, we define the function $g(x)$ introduced in Eq. (9) as the average value of the eddy viscosities at the outer edges of the viscous layer; i.e., $g(x) = [e_{0,+}(x) + e_{0,-}(x)]/2$. This value is used for both the suction- and pressure-surface boundary-layer calculations as well as for the wake calculation.

Solution Procedure

A solution for the entire flowfield is determined by matching the solutions to the inviscid and viscous equations. Strong-interaction effects are determined using a global iteration procedure. Here the displacement thickness distribution $\delta^n(x)$ for the $(n+1)$ iteration is prescribed, the inviscid and viscous equations are solved to determine an intermediate displacement thickness distribution $\delta^{n+\frac{1}{2}}(x)$, and the $(n+1)$ distribution $\delta^{n+1}(x)$ is estimated according to the relation

$$\delta^{n+1}=\omega\delta^{n+\frac{1}{2}}+(1-\omega)\delta^n \tag{20}$$

where ω is a relaxation factor. This process is repeated until the maximum value of $|\delta^{n+1}(x)-\delta^n(x)|/\delta^{n+1}(x)$ over the strong-interaction domain satisfies some specified convergence criterion.

A semi-inverse global iteration procedure[15] was applied in our earlier work[1,2] to predict laminar attached and separated trailing-edge flows. This procedure is generally satisfactory, giving reasonable convergence rates for attached flows, but it requires a prohibitive number of iterations using substantial underrelaxation ($\omega<1$) to achieve converged solutions for separated flows. Also, stability problems (see Ref. 16) may be encountered when displacement thickness gradients are large and/or streamwise mesh spacings are small. Thus, we have implemented a quasi-simultaneous coupling procedure introduced by Veldman[3] and applied recently in the calculation of several strong-interaction flowfields.[4,9,10,17] With this procedure, the viscid and inviscid solutions are coupled locally at each level of the global iteration. As a result, the convergence rate of the global viscid/inviscid iterations is enhanced considerably over that achieved with semi-inverse iteration. Details on the present implementation of the quasi-simultaneous procedure are given later, but first we outline briefly the numerical methods used to solve the equations governing the flows in the inviscid and viscous regions.

Inviscid Surface Pressure

We require numerical solutions for the first-order inviscid surface pressure and the viscous displacement thickness over a strong-interaction solution interval extending from $x=x_I$ to $x=x_F$. To evaluate the inviscid pressure, the first integral on the right-hand side of Eq. (5) is here approximated using trapezoidal-rule quadrature, i.e.,

$$\int_{x_{IB}}^{x_{IE}}\frac{D_T'(\zeta)}{x_i-\zeta}\,d\zeta\approx\sum_{j=IB}^{IE-1}D_T'(\bar{x}_j)\,\frac{x_{j+1}-x_j}{x_i-\bar{x}_j} \tag{21}$$

where i and j are streamwise mesh points indices, IB and IE refer to the mesh stations at the beginning and end of the strong-interaction solutions domain, respectively (i.e., at x_I and x_F), and $\bar{x}_j=(x_{j+1}+x_j)/2$. This discrete representation is accurate to first-order in Δx, whereas the representation used in Refs. 1 and 2 is second-order accurate. However, as discussed in Ref. 3, the use of a first-order accurate discretization allows for an efficient implementation of the quasi-simultaneous coupling procedure. Although neglected here, contributions to the local (at $x=x_i$) pressure due to thickness effects from upstream ($0<\zeta<x_I$) and downstream (at $\zeta>x_F$) of the strong-interaction region can be determined by analytical or numerical integration, depending upon the assumed functional form of $D_T(x)$. The discrete approximations used to calculate the second integral in Eq. (5) and the pressure jump due to wake curvature are identical to those described in our earlier work.[1,2]

Viscous Layer

The viscous-layer equations are solved in an inverse fashion; i.e., the pressure is determined in terms of the displacement thickness. Solutions for the boundary layers on the upper and lower surfaces of the airfoil and for the wake are determined by marching in the streamwise direction from an upstream station where the velocity profile is obtained from a direct boundary-layer solution. The continuity and momentum equations are replaced by a set of linear algebraic equations using a finite-difference approximation in which the nonlinear terms in the momentum equation at the $(n+1)$ iteration are linearized about the solution at the previous, (nth), iteration and the ξ and η derivatives are replaced by one-sided and central difference expressions respectively. An upwind differencing scheme is used for the ξ derivatives; i.e., backward differencing is used if $F>0$ and forward differencing if $F<0$.

The resulting set of linear difference equations is solved using a superposition technique; i.e., the dependent variables F and V are decomposed (e.g., $F=\beta F_I+F_{II}$) so that two uncoupled sets of linear algebraic equations are obtained. The components of F and V are related through a viscous constraint relation,

$$\beta=(I_b/2I_a)\left\{\left[1+4I_a\left(I_c-\frac{\rho_e u_e\delta}{\sqrt{2\xi/Re}}\right)\Big/I_b^2\right]^{\frac{1}{2}}-1\right\} \tag{22}$$

which is obtained from the definition of the displacement thickness, Eq. (15), after solving the resulting quadratic equation for β and eliminating the extraneous solution. The quantities I_a, I_b, and I_c are given by

$$I_a=\frac{\gamma-1}{2}(M_e)^2\int_0^\infty F_I^2\,d\eta \tag{23a}$$

$$I_b=\int_0^\infty[1+(\gamma-1)(M_e)^2F_{II}]F_I\,d\eta \tag{23b}$$

$$I_c=\int_0^\infty\left[1-F_{II}+\frac{\gamma-1}{2}(M_e)^2(1-F_{II}^2)\right]d\eta \tag{23c}$$

The solution for an asymmetric viscous wake is obtained by treating the upper and lower sides of the wake simultaneously. A boundary condition is imposed on F at each edge and on V at the reference streamline. At the trailing edge of an asymmetric airfoil, the upper- and lower-surface values of ξ and η will generally differ. Therefore the trailing-edge velocity profile on the lower surface of the airfoil is expressed in terms of the upper-surface variables (ξ_+,η_+), and these are used to continue the viscous-layer solution into the wake.

Quasi-Simultaneous Coupling Procedure

The quasi-simultaneous procedure requires a local coupling of the inviscid and viscid solutions to determine the intermediate displacement thickness distribution ($\delta^{n+\frac{1}{2}}$) at each level of the global iteration procedure. This coupling can be achieved by working with the two relations, Eqs. (13) and (22), for the pressure gradient paramater β. Using the relations of linearized potential flow theory, the pressure gradient parameter can be written in the form

$$\beta=-2\xi\left(1+\frac{(\gamma-1)M_\infty^2}{2}\right)\frac{dp_D}{d\xi} \tag{24}$$

We introduce the integer index k to assist in describing the local coupling procedure, and set

$$k=2(i-IB)+1,\quad i=IB,IB+1,\ldots,IT \tag{25a}$$

$$k=2(i-IB)+2,\quad i=IB,IB+1,\ldots,IT \tag{25b}$$

to identify streamwise mesh stations on the upper and lower surfaces of the airfoil, respectively, and

$$k = i - IT + 2(IT - IB) + 2, \quad i = IT+1, IT+2, \ldots, IE \tag{25c}$$

to identify stations in the wake. Here $i = IT$ refers to the station at the trailing-edge point of the airfoil. The viscid/inviscid interaction solution at the nth global iteration level is obtained by marching from $k=3$ to $k = KE = IE - IT + 2(IT - IB) + 2$. Thus for $IB+1 \le i \le IT$ the solution at $\xi = \xi_i$ is first determined on the upper surface of the airfoil and then on the lower surface, and for $IT < i \le IE$ the solution is determined for the complete wake. Conditions at the beginning of the strong-interaction solution domain (i.e., at $k = 1,2$) are fixed and obtained as a direct solution of the boundary-layer equations for a prescribed inviscid pressure gradient.

A discrete approximation to Eq. (24) can be written in the form

$$\beta_k = \sum_{j=1}^{k-1} \alpha_{kj}\delta_j^{n+1/2} + \alpha_{kk}\delta_k^{n+1/2} + \sum_{j=k+1}^{KE} \alpha_{kj}\delta_j^n + Q_k, \quad k = 3, \ldots, KE \tag{26}$$

where the coefficients $\alpha_{k,j}$ and Q_k are known and depend upon the difference approximations used to evaluate the inviscid pressure p_D [i.e., Eq. (5)] and pressure gradient $dp_D/d\xi$. The δ_j^n are prescribed for all j, and the $\delta_j^{n+1/2}$ for $j<k$ are determined by the current [i.e., the $(n+1)$] marching solution. Thus the only unknowns in Eq. (26) are β_k and $\delta_k^{n+1/2}$. The second relationship needed to solve for these two unknowns is provided by Eq. (22) evaluated at k, $n+1/2$. Although this local coupling of the inviscid and viscous solutions requires more computational effort at each iteration level than that needed for a semi-inverse calculation, if properly implemented it leads to a significant reduction in the number of global iterations required to determine a converged strong-interaction solution.

Once updated values of δ (i.e., $\delta_j^{n+1/2}$) are obtained, corresponding values of the inviscid flow properties (p_D, u_e, etc.) are determined in terms of the $\delta_j^{n+1/2}$ at $j=1,\ldots,k$, and the δ_j^n at $j=k+1,\ldots,KE$, and the viscous-layer variables F and V at station k are determined in terms of β. With this information, the marching procedure can be continued downstream. For symmetric flows, the foregoing procedure is simplified considerably since solutions are only required in either the upper or lower half-plane.

As pointed out by Davis[4] and Veldman,[9] the matrix of influence coefficients, α_{kj} in Eq. (26), should be diagonally dominant. Since the second-order accurate discretization used in Refs. 1 and 2 for the symmetric component of the inviscid pressure does not yield a diagonally dominant matrix of influence coefficients, we have adopted the first-order accurate approximation given by Eq. (21). In addition, the quantities D_T' and D_C' in Eq. (5) and the pressure gradient $dp_D/d\xi$ in Eq. (24) have been evaluated using first-order accurate backward-difference approximations. Most of the solutions obtained in the present study converged using a relaxation factor of one. However, underrelaxation with $\omega = 0.5$ was required for several of the calculations in which a one-sided flow separation occurred.

Numerical Results

The foregoing procedures have been applied to predict turbulent mean flows in the trailing-edge/near-wake region first for a family of model airfoils and then for the airfoil studied experimentally by Viswanath and Brown.[5] In the first case, the airfoil surfaces are located at

$$y_\pm(x) = h_\pm(x) = \pm D_{T,A}(x) + D_{C,A}(x), \quad x \in [0,1] \tag{27}$$

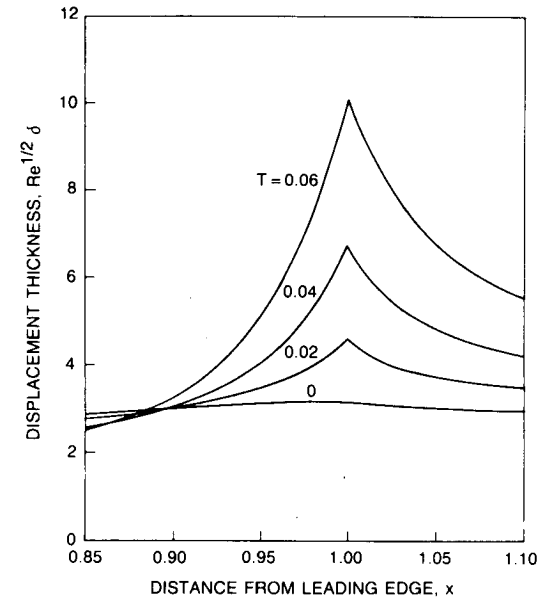

a) Displacement thickness distributions.

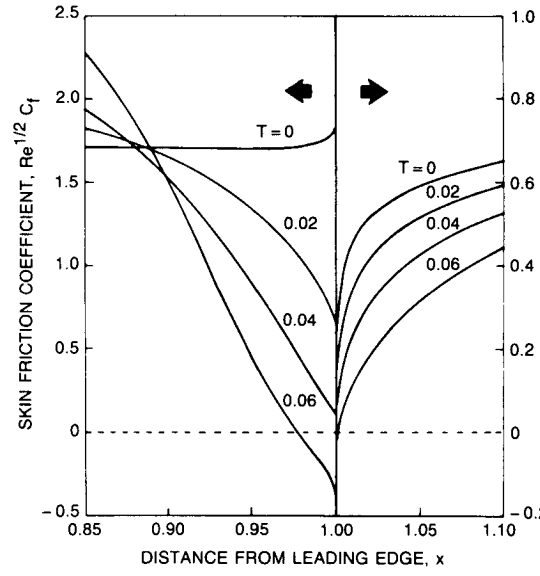

b) Skin-friction and wake centerline velocity distributions.

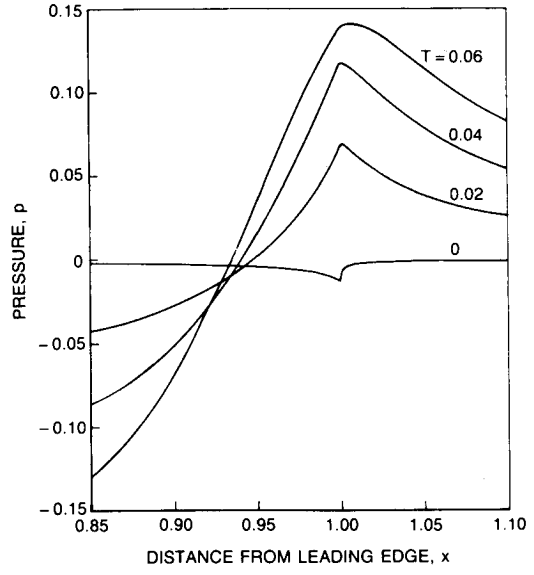

c) Pressure distributions.

Fig. 2 Symmetric trailing-edge flow: effect of airfoil thickness; $M_\infty = 0.7$, $Re = 10^6$, $\alpha = 0$.

where $2D_{T,A}$ defines the airfoil thickness distribution and $D_{C,A}$ defines the location of the airfoil camber line. Here $D_{T,A}$ is given by

$$\begin{aligned} D_{T,A}(x) &= T/2, && 0 \le x < x_c \\ &= T/2 - R + \sqrt{R^2 - (x - x_c)^2}, && x_c \le x \le 1 \\ &= 0, && x > 1 \end{aligned} \tag{28}$$

where T is the maximum thickness of the airfoil, $R = T^{-1}[T^2/4 + (1-x_c)^2]$ is the radius of curvature of the circular-arc trailing-edge section, and x_c is the point at which these circular-arc sections are joined to the flat forward sections of the airfoil. For the present purpose of analyzing local strong-interaction effects at the trailing edge, there is no need to specify closure at the airfoil leading edge. The antisymmetric part of the airfoil (i.e., the camber distribution) is determined from a prescribed pressure jump $[p_A^A(x)]$ across the airfoil which is assumed to be constant upstream of the point $x = x_c$ and equal to that acting on a flat plate inclined at an angle α relative to the uniform stream for $x_c \le x \le 1$; i.e.,

$$\begin{aligned} [P_A^A(x)] &= \frac{-2\alpha}{(1-M_\infty^2)^{1/2}} \frac{(1-x_c)^{1/2}}{x_c^{1/2}}, && 0 < x < x_c \\ &= \frac{-2\alpha}{(1-M_\infty^2)^{1/2}} \frac{(1-x)^{1/2}}{x^{1/2}}, && x_c \le x \le 1 \\ &= 0, && x > 1 \end{aligned} \tag{29}$$

The location of the airfoil camber line can then be determined by integration after setting $[p_D] = [p_A^A]$ and $D_C = D_{C,A}$ in Eq. (7) and $D_{C,A}(1) = 0$.

Numerical results will be presented for symmetric ($\alpha = 0$) and asymmetric high-subsonic ($M_\infty = 0.7$) turbulent flows at $Re = 10^6$ to illustrate the effects of airfoil thickness and loading on trailing-edge flow behavior. Note that although our results for the displacement thickness and skin-friction distributions are presented in terms of $Re^{1/2}\delta$ and $Re^{1/2}C_f$ respectively, this is not meant to imply that δ and C_f scale with the square root of the Reynolds number for turbulent mean flows. For the present calculations, the value of x_c has been set at 0.75. The viscous-layer solution domain extends out to $\eta = 11$ in the normal direction. This, together with the use of the scaling function $g(x)$ in Eq. (9), places the outer boundary of the computational region sufficiently far from the airfoil and reference wake streamline to enable the viscous effects to be captured properly at all streamwise locations. The distribution of points in the normal direction has been chosen so that $y^+ = yu_\tau/\mu$, where u_τ is the maximum value of the friction velocity, is less than one at the first grid point off the surface. However, for separated flows it can be difficult to achieve a converged solution unless y^+ is set to be between one and three. A similar problem was observed by Chang et al.[18] and may be associated with the evaluation of the friction velocity. For the boundary-layer calculations, a total of 41 normal grid lines have been used with stretching applied to give the desired value of y^+ at the first line. The same stretching has been used for both upper- and lower-surface boundary layers. In the wake, 81 normal grid lines are used. In addition, a total of 81 variably spaced mesh lines are used in the streamwise direction with 51 lines intersecting the airfoil. These lines are clustered in the vicinity of the trailing edge, with the minimum spacing taken to be on the order of $Re^{-3/5}$ (see Ref. 18). Turbulent boundary-layer profiles at the initial station have been computed for a prescribed inviscid pressure gradient, neglecting the ξ derivatives there. Global iterations have been repeated until the maximum relative change in displacement thickness over the strong-interaction domain is less than 1×10^{-6}. With this stringent criterion, 40–50 global iterations with $\omega = 1$ are generally required to achieve converged attached-flow solutions, and as many as 200–300 iterations using underrelaxation are required for flows in which a one-sided separation occurred. Computation times for the grid and convergence criterion previously described were on the order of 30 min on an Apollo DN460 workstation for the attached-flow cases presented here.

Symmetric Trailing-Edge Flows

Results illustrating the effect of airfoil thickness T on the flow in the trailing-edge region are shown in Fig. 2, where values of T equal to 0 (flat-plate airfoil), 0.02, 0.04, and 0.06 have been considered. For the double-circular-arc trailing-edge profiles ($T > 0$), the viscous displacement thickness (Fig. 2a) increases rapidly up to the trailing-edge point and then decreases less rapidly along the wake. The net effect is a smoothing of the effective shape of the airfoil and wake as seen by the outer inviscid flow. The skin-friction coefficient C_f (at $\eta = 0$) and wake centerline velocity distributions u_W (Fig. 2b) indicate that the flow separates upstream of the trailing edge for $T = 0.06$. Note that in this case there is an abrupt decrease in the skin friction just before the trailing edge and the reverse-flow region terminates just aft of the trailing edge. These features could not be resolved without the use of a very fine grid in the immediate vicinity of the trailing edge. The pressure acting on the thick airfoils (Fig. 2c) increases with x up to the trailing edge and into the near wake and then gradually drops to its freestream value downstream. The differences between the flow behaviors for the flat-plate and the thick airfoils are caused by the closure of the latter in finite trailing-edge angles. This closure causes the flow to decelerate as it approaches the trailing edge, leading to a thickening of the viscous layer, a decrease in skin friction, and an increase in surface pressure.

Asymmetric Trailing-Edge Flows

Asymmetric flow results for cambered flat-plate ($T = 0$) and 2% thick ($T = 0.02$) airfoils are presented in Figs. 3 and 4, respectively. The camber distributions are defined by prescribing the loading parameter α in Eq. (29). The effects of viscous displacement and wake curvature on the pressure distribution in the trailing-edge region of a cambered airfoil are depicted in Fig. 5.

For the cambered flat plates, the displacement thickness (Fig. 3a) of the suction-surface boundary layer increases, while that of the pressure-surface boundary layer decreases, but to a lesser extent, with an increase in airfoil loading. The net effect is a thickening of the displacement body in the trailing-edge region with increasing loading. For $\alpha \neq 0$, the skin-friction coefficient (Fig. 3b) generally decreases along the suction surface, and increases along the pressure surface with increasing distance along the airfoil. Just upstream of the trailing edge, the flow along the pressure surface accelerates due to the relief of the no-slip condition in the near wake. On the suction surface, the flow accelerates just before the trailing edge at lower loadings, but at the higher loadings the decelerating effect of the adverse pressure gradient is stronger than the accelerating effect due to the relief of the no-slip condition. Airfoil loading appears to have little impact on the wake streamline velocity, at least for the attached flows considered in Fig. 3. Finally, the pressure difference across the airfoil increases with increasing loading (Fig. 3c). In the immediate vicinity of the trailing edge, negative loading is observed as a result of the wake curvature effect. In the wake, the pressure rises rapidly with increasing streamwise distance to the freestream value downstream.

A comparison of the results for the 2% thick airfoil with those for the cambered flat-plate airfoils, presented in Fig. 4, reveals that airfoil thickness has a substantial effect on the

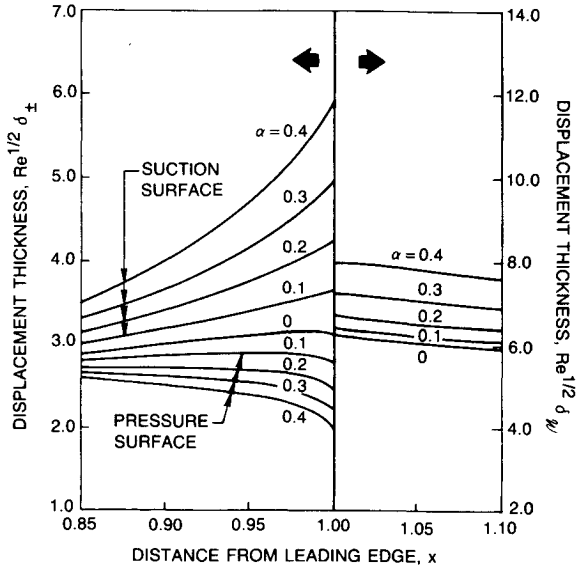

a) Displacement thickness distributions.

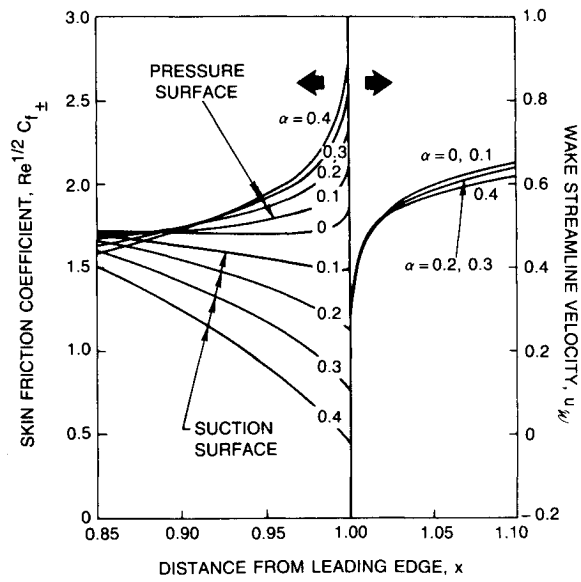

b) Skin-friction and wake streamline velocity distributions.

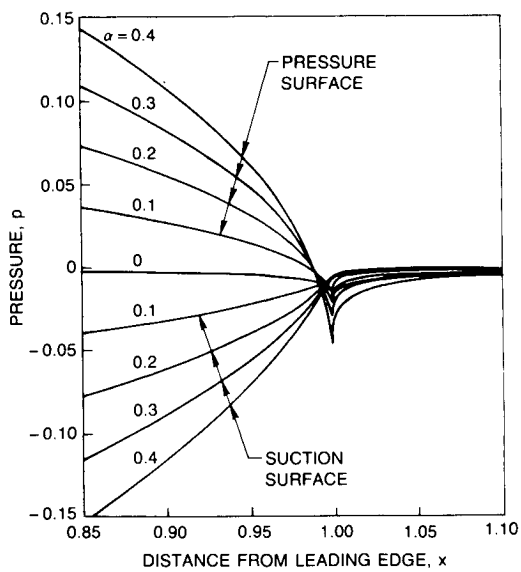

c) Pressure distributions.

Fig. 3 Asymmetric trailing-edge flow: effect of airfoil loading; $M_\infty = 0.7$, $Re = 10^6$, $T = 0$.

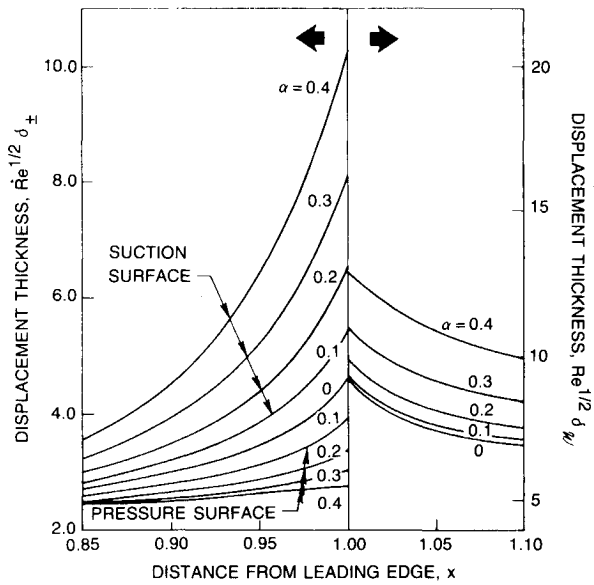

a) Displacement thickness distributions.

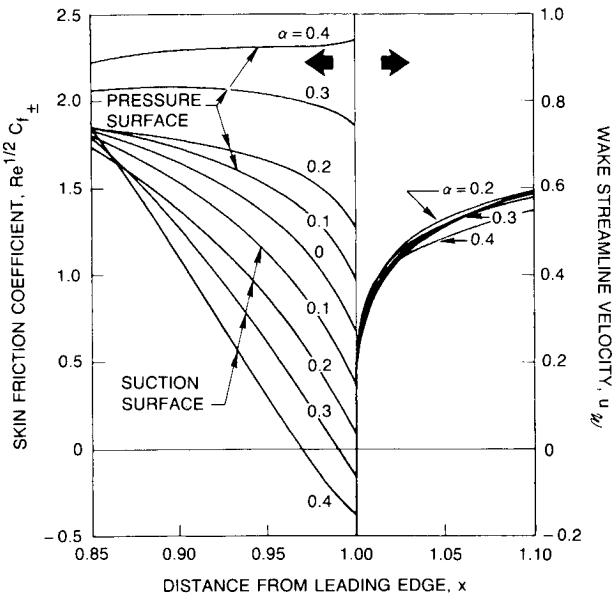

b) Skin-friction and wake streamline velocity distributions.

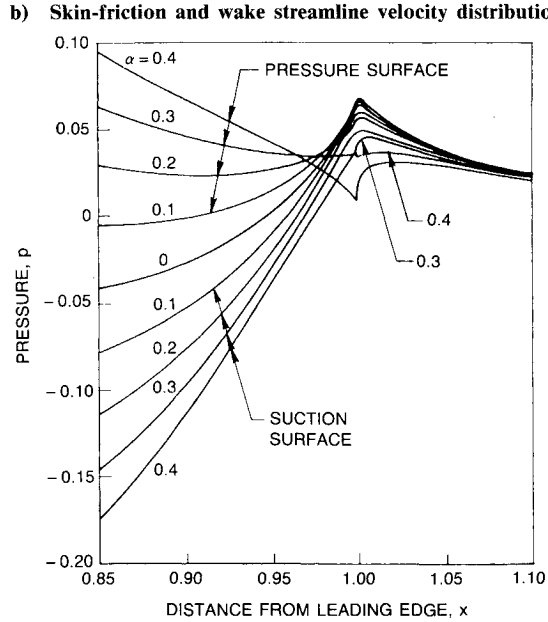

c) Pressure distributions.

Fig. 4 Asymmetric trailing-edge flow: effect of airfoil loading for a 2% thick airfoil; $M_\infty = 0.7$, $Re = 10^6$, $T = 0.02$.

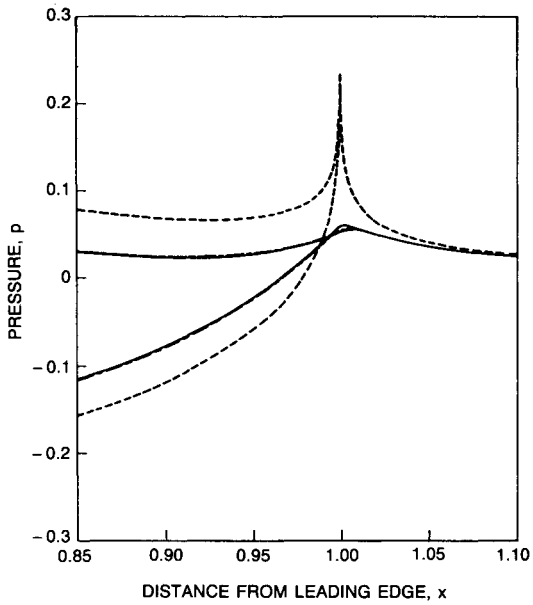

Fig. 5 Viscous effects on the pressure in the trailing-edge region of a 2% thick airfoil; $M_\infty = 0.7$, $Re = 10^6$, $\alpha = 0.2$, $T = 0.02$. - - - airfoil, — - — airfoil + viscous displacement, —— airfoil + viscous displacement + wake curvature.

flow behavior in the trailing-edge region of a loaded airfoil. Again, this difference is due primarily to the decelerating effect of thick-airfoil closure. In particular, the displacement thicknesses (Fig. 4a) of the boundary layers on both the pressure and suction surfaces of the 2% thick airfoils increase with distance along the airfoil, while for the cambered flat plates, the displacement thickness of the pressure-surface boundary layer decreases with increasing distance just upstream of the trailing edge. The skin-friction coefficients (Fig. 4b) for the 2% thick airfoils generally decrease on the suction surface and, when the loading is not too high, on the pressure surface as the trailing edge is approached. In addition, small reverse-flow regions adjacent to the suction surface are predicted for $\alpha = 0.3$ and 0.4. The surface pressures in the trailing-edge region ($x > 0.85$) for the 2% thick airfoils (Fig. 4c) are generally lower than those for the corresponding cambered flat plates. The level at the trailing edge is greater than the freestream pressure in contrast to the lower than freestream pressure observed at the trailing edge of the cambered flat plates. In the near wake, the pressure returns to the freestream level, but at a relatively slow rate.

As illustrated in Fig. 5 for a 2% thick airfoil with $\alpha = 0.2$, viscous effects cause a significant reduction in the airfoil loading that would be predicted from inviscid considerations alone. The viscous displacement effect tends to uncamber the airfoil, thereby reducing the loading. In general, both displacement and wake curvature effects tend to decrease the loading on the airfoil, but for the example considered, the wake curvature effect is much smaller than that of viscous displacement. This is evident in Fig. 5, where the calculated inviscid surface pressure distribution is shown along with the surface pressure that results when viscous displacement effects are considered, and finally, when both viscous displacement and wake curvature effects are taken into account.

Effect of Mach Number and Reynolds Number

Calculations have also been performed to determine the effect of variations in the Mach number and the Reynolds number of the turbulent mean flow in the vicinity of the trailing edge of a loaded (with $\alpha = 0.3$) 2% thick airfoil. In one study, the Reynolds number has been held at 10^6 and Mach numbers of 0.5, 0.7, and 0.8 are considered. In the other, the Mach number has been held at 0.7 and Reynolds

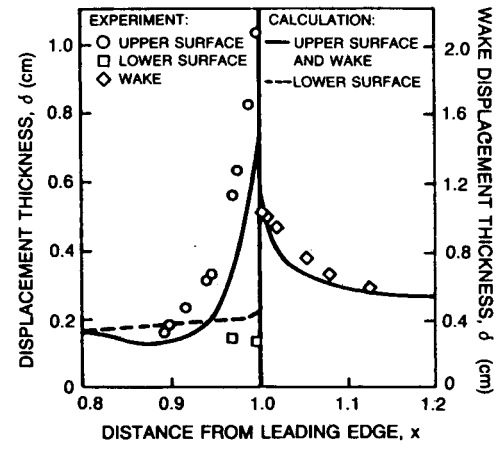

a) Displacement thickness distributions.

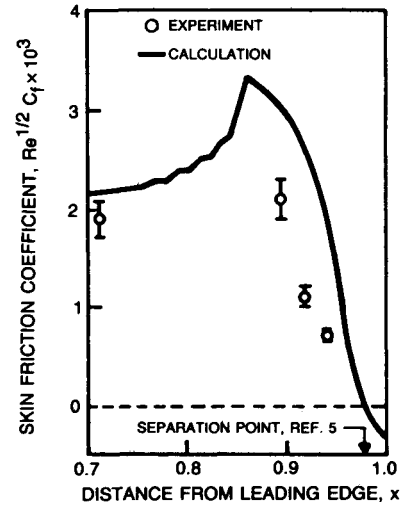

b) Skin-friction distributions.

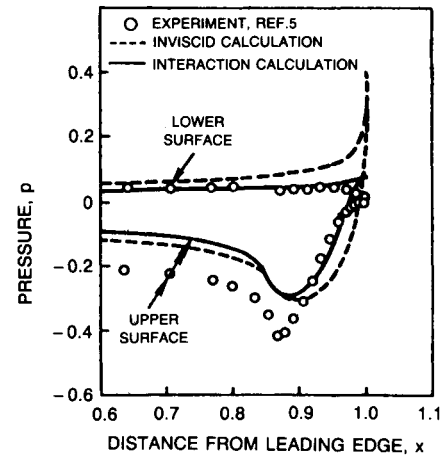

c) Pressure distributions.

Fig. 6 Analytical/experimental comparison; $M_\infty = 0.7$, $Re = 40 \times 10^6$.

numbers of 10^5, 10^6 and 10^7 are considered. We find that an increase in the Mach number leads to an increase in the displacement thickness and an uncambering of the airfoil and therefore a decrease in the airfoil loading in the trailing-edge region. At all three Mach numbers, the flow separates from the suction surface just upstream of the trailing edge and reattaches at the trailing edge. The streamwise extent of the reverse-flow region increases with increasing Mach number and spans approximately 2% of the airfoil chord at $M_\infty = 0.8$.

An increase in the Reynolds number at $M_\infty = 0.7$ leads to an increase in displacement body thickness and camber and therefore an increase in airfoil loading, except in the immediate vicinity of the trailing edge. The flows at $Re = 10^5$ and $Re = 10^6$ separate from the suction surface, and the streamwise extent of the reverse-flow region is approximately 4.5 and 1.2% of the blade chord, respectively. The flow at $Re = 10^7$ remains attached to the airfoil. This trend is in contrast to laminar flow predictions, which indicate that the flow is more likely to separate at a higher Reynolds number.

Analytical/Experimental Comparison

Theoretical predictions have been determined for the flow past an airfoil for which benchmark experimental data exists.[5] The airfoil is essentially a thickened flat plate. The upper and lower surfaces join in a wedge-shaped leading edge, and the trailing-edge section consists of a flat lower surface and a circular-arc upper surface that terminate in a finite wedge angle of 20.4 deg. The airfoil geometry is defined in Ref. 5. For the calculations, a slight modification to the experimental geometry has been introduced at the leading edge, but this has a negligible effect on the calculated flow near the trailing edge. The experiment was conducted at a freestream Mach number of 0.7 and a Reynolds number of 40 million. Unfortunately, the experiment was conducted in a wind tunnel with a height to airfoil chord ratio of 0.4, while our theoretical predictions apply to an airfoil in an unbounded flow. Therefore a significant difference between the experimentally measured and numerically calculated loadings occurs. The difference is due to wind tunnel blockage effects and is consistent with the amount of blockage present in the experiment. In addition, in both the experiment and the prediction the flow reaches a Mach number very close to one on the upper surface near the trailing edge. The presence of nearly sonic velocity along with the relatively large wedge angle at the trailing edge makes it difficult to model this flow with classical thin-airfoil theory. Despite these difficulties, qualitative agreement with the experimental data has been achieved and provides some verification of the present analytical model.

The initial boundary-layer profile for the calculation is specified at $x = 0.05$ and is assumed to be that for laminar flow past a thin flat plate. No information on the location of transition is provided in Ref. 5; therefore, instantaneous transition to turbulent flow has been assumed to occur between the first and second stations on the airfoil. A region of weak viscid/inviscid interaction is assumed over the forward portion of the airfoil extending to $x \sim 0.5$. In this region, the viscous-layer solution has been marched with the pressure gradient imposed by the inviscid solution (direct mode). Downstream of the weak-interaction region, the viscous calculation is continued in the inverse (strong-interaction) mode to $x = 1.5$. The strong-interaction solution has been converged until the maximum relative change in the displacement thickness is less than 10^{-3}. The grid in the strong-interaction region consists of 131 points in the streamwise direction, with 68 points along the airfoil surface and 141 points in the normal direction across the wake (71 points normal to each surface on the airfoil). The streamwise mesh spacing at the trailing edge, Δx, is equal to 0.00085.

The results of the present calculation are given in Fig. 6, along with the experimental data of Ref. 5. The displacement thickness distributions on the airfoil surfaces and in the wake are shown in Fig. 6a. Qualitative agreement between the calculated results and the measurements is observed, with the displacement thickness somewhat underpredicted on the upper and overpredicted on the lower surface of the airfoil. Although the experimental data for the skin friction is sparse, the agreement between the predictions and the available data is reasonable (Fig. 6b). The mild oscillations observed in the calculated results upstream of the peak in the skin friction are believed to be due to insufficient streamwise resolution in that region. Although perhaps fortuitous, the predicted and measured separation point location agree very well. The experimentally measured pressure distribution is presented in Fig. 6c, along with two calculated pressure distributions—one based on purely inviscid considerations and the other determined as a strong viscous/inviscid interaction solution. The impact of viscous effects on the airfoil loading and on the removal of the pronounced peak in the inviscid pressure at the trailing edge is clearly evident from the calculated results. The measured and predicted pressure distributions are in qualitative agreement, except in the immediate vicinity of the trailing edge. A possible source for the disagreement in the behavior of the pressure near the trailing edge is the use of a turbulence model in the present calculation which is not adequate for flows with strong adverse pressure gradients and boundary-layer separation.

Concluding Remarks

An analytical procedure based on finite Reynolds number interacting boundary-layer theory has been developed for predicting the subsonic turbulent mean flow in the trailing-edge and near-wake region of an airfoil. A quasi-simultaneous coupling procedure, which is characterized by a local coupling of the viscous and inviscid solutions at each global viscid/inviscid iteration level, has been employed to provide a relatively efficient solution technique for flows with strong viscid/inviscid interactions. The present analysis can provide a useful basis for future studies on turbulent mean-flow behavior, including separation phenomena, in the vicinity of airfoil trailing edges. In particular, it will allow detailed investigations to be made on the effects of airfoil geometry, turbulence model, oncoming boundary-layer profiles, etc., on the flow in the trailing-edge/near-wake region of an airfoil.

Numerical results have been presented for symmetric and asymmetric turbulent flows. The behavior of the flow in the airfoil trailing-edge and near-wake region, as the parameters governing the airfoil thickness and camber are varied, has been demonstrated through a systematic parametric study. For the airfoil geometries and flow conditions considered here, wake curvature is found to have a much smaller effect on the airfoil and near-wake pressures than does viscous displacement. Both effects lead to a reduction in the lift that would be predicted by a purely inviscid analysis. Turbulent mean flow separations have been predicted, but they occur under much more severe conditions (i.e., greater airfoil thickness and loading and higher flow Mach number) than are required to separate laminar flows. In addition, a calculation has been performed to allow comparison with experimental data in an effort to validate the present approach. The numerical results are found to be in qualitative agreement with the experimental data, with most of the differences traceable to the facts that the experiment was conducted in a wind tunnel and the calculation has been performed for an unbounded flow.

An important point to recognize when computing turbulent flows is the dependence of the mean-flow solution upon the turbulence model imposed. Differences in calculated results can be expected when using different turbulence models, particularly when strong adverse pressure gradients and/or boundary-layer separations are present. In the future, the use of wall functions, within the present approach, to represent the turbulent mean flow close to the airfield surface (see Ref. 19) should be considered to provide a more efficient calculation procedure for practical applications. In addition, a fully nonlinear inviscid flow representation would permit the analysis of highly-loaded airfoils. For such applications, it may be necessary to provide a method for including wake curvature as a strong viscid/inviscid interaction.

Acknowledgments

This research was sponsored by the Naval Air Systems Command under Contract N00014-83-C-0430. The assistance provided by Dr. R. P. Shreeve, NASC Program Manager for this contract, is gratefully acknowledged.

References

[1]Vatsa, V. N. and Verdon, J. M., "Viscous/Inviscid Interaction Analysis of Asymmetric Trailing-Edge Flows," *Numerical and Physical Aspects of Aerodynamic Flows*, edited by T. Cebeci, Springer-Verlag, New York, 1984, pp. 205–221.

[2]Vatsa, V. N. and Verdon, J. M., "Viscid/Inviscid Interaction Analysis of Separated Trailing-Edge Flows," *AIAA Journal*, Vol. 23, April 1985, pp. 481–489.

[3]Veldman, A. E. P., "New, Quasi-Simultaneous Method to Calculate Interacting Boundary Layers," *AIAA Journal*, Vol. 19, Jan. 1981, pp. 79–85.

[4]Davis, R. T., "A Procedure for Solving the Compressible Interacting Boundary Layer Equations for Subsonic and Supersonic Flows," AIAA Paper 84-1614, June 1984.

[5]Viswanath, P. R. and Brown, J. L., "Separated Trailing-Edge Flow at a Transonic Mach Number," *AIAA Journal*, Vol. 21, June 1983, pp. 801–807.

[6]Smith, F. T., "Interacting Flow Theory and Trailing-Edge Separation—No Stall," *Journal of Fluid Mechanics*, Vol. 131, June 1983, pp. 219–250.

[7]Smith, F. T., "On the High Reynolds Number Theory of Laminar Flows," *IMA Journal of Applied Mathematics*, Vol. 28, May 1982, pp. 207–281.

[8]Elliott, J. W. and Smith, F. T., "Separated Supersonic Flow Past a Trailing Edge at Incidence," *Computers and Fluids*, Vol. 14, No. 2, 1986, pp. 109–116.

[9]Veldman, A. E. P., "The Calculation of Incompressible Boundary Layers with Strong Viscous-Inviscid Interaction," *AGARD Symposium on Computation of Viscous-Inviscid Flows*, AGARD-CPP-29, Chap. 12, 1980.

[10]Veldman, A. E. P. and Lindhout, J. P. F., "Quasi-Simultaneous Calculations of Strongly Interacting Viscous Flow," *Numerical and Physical Aspects of Aerodynamic Flows III*, edited by T. Cebeci, Springer-Verlag, New York, 1986.

[11]Melnik, R. E. and Brook, J. W., "The Computation of Viscid/Inviscid Interaction on Airfoils with Separated Flow," *Numerical and Physical Aspects of Aerodynamic Flows III*, edited by T. Cebeci, Springer-Verlag, New York, 1986.

[12]Cebeci, T., Clark, R. W., Chang, K. C., Halsey, N. D., and Lee, K., "Airfoils with Separation and the Resulting Wakes," *Numerical and Physical Aspects of Aerodynamic Flow III*, edited by T. Cebeci, Springer-Verlag, New York, 1986.

[13]Cebeci, T. and Smith, A. M. O., *Analysis of Turbulent Boundary Layers*, Academic Press, New York, 1974, pp. 211–239.

[14]Cebeci, T., Thiele, F., Williams, P. G., and Stewartson, K., "On the Calculation of Symmetric Wakes I. Two-Dimensional Flows," *Numerical Heat Transfer*, Vol. 2, 1979, pp. 35–60.

[15]Carter, J. E., "A New Boundary Layer Interaction Technique for Separation Flows," AIAA Paper 79-1450, July 1979.

[16]Wigton, L. B. and Holt, M., "Viscous-Inviscid Interaction in Transonic Flows," AIAA Paper 81-1003, June 1981.

[17]Edwards, D. E. and Carter, J. E., "A Quasi-Simultaneous Finite Difference Approach for Strongly Interacting Flow," *Third Symposium on Numerical and Physical Aspects of Aerodynamic Flows III*, edited by T. Cebeci, Springer-Verlag, New York, 1986.

[18]Chang, K. C., Bui, M. N., Cebeci, T., and Whitelaw, J. H., "The Calculation of Turbulent Wakes," *AIAA Journal*, Vol. 24, Feb. 1986, pp. 200–201; also, Rept. ME-84-3, California State Univ., Long Beach, CA, Sept. 1984.

[19]Viegas, J. R., Rubesin, M. W., and Horstman, C. C., "On the Use of Wall Functions as Boundary Conditions for Two-Dimensional Separated Compressible Flows," AIAA Paper 85-0180, Jan. 1985.